Semiconductor physics

Determination of crystallization conditions of Ge/GaAs heterostructures in scanning LPE method

V.V. Tsybulenko, S.V. Shutov, S.Yu. Yerochin

V. Lashkaryov Institute of Semiconductor Physics, NAS of Ukraine,
76/78, Zavodska str., 73008 Kherson, Ukraine
E-mail: shutov_sv@isp.kiev.ua

Abstract. We carried out the modelling of separate technological stages of scanning liquid phase epitaxy (SLPE) technique: wetting the substrate by the solution-melt using Ampere force, growing the epitaxial layer during a short-time contact between the substrate and solution-melt, and removing the solution-melt from the substrate using Ampere force as well. The modelling was carried out for the case of Ge layers growing on GaAs substrate from Ga-Ge solution-melt at the temperature 500 °C. We have ascertained that the Peltier effect and Joule heating practically have no effect on the growth pattern and under certain conditions could be even diminished. The influence of electromigration and convection in the solution-melt can be neglected. It has been shown that the basic technological parameters of SLPE process are as follows: the initial temperatures and sizes of the substrate and the growing vessel, the conditions of heat removal from the substrate back side and the time of the process. It has been also shown that the major contribution into the epitaxial layer thickness distribution over the substrate surface has been made by the heat distribution in the cooled substrate.

Keywords: scanning liquid phase epitaxy, Ampere force, heterostructures, thin films.

https://doi.org/10.15407/spqeo23.03.294
PACS 81.15.Lm, 81.15.-z, 81.15.Aa

Manuscript received 12.12.19; revised version received 28.05.20; accepted for publication 10.09.20; published online 22.09.20.

1. Introduction

To date, basic methods to fabricate various heterostructures for device applications are metal-organic vapor phase epitaxy, metal organic chemical vapor deposition and molecular beam epitaxy [1-3]. Many of these deposition techniques are difficult to apply over a large area and are expensive due to complexity of the apparatus used. In addition, there is the problem of a substrate selection, since for many common substrates there is a large mismatch in the lattice constants and thermal expansion coefficients. Due to the difference in lattice constants, it is difficult to homogenously deposit films onto a substrate. Also, one can find the works on heterostructures fabrication by using the liquid phase epitaxy (LPE) methods [4-7]. It is well known that those techniques are more simple and cheap as compared with the above mentioned techniques. So, they should have been widely used for heterostructure fabrication, particularly for photovoltaic cells (PC) [8, 9]. However, the LPE techniques possess a series of drawbacks that limit their potential [10].

In [11], we presented the method that allowed to eliminate some of the LPE disadvantages. This method is called as scanning LPE technique (SLPE). This method is promising, as it allows to eliminate the influence of the following drawbacks: temperature instability at the growth interface due to thermal inertia of the heater, dragging solution-melts between different growing vessels and diffusion of a solution-melt or an epitaxial layer components into the solid phase. The technique allows to produce a short-time contact between a substrate and a solution-melt only during the growth of the epitaxial layer and on the growth completion the substrate is cleansed of the solution-melt immediately. Segmental contact between the substrate and solution-melt makes it possible to grow epitaxial layers on the very large area substrates, which is useful for the PC fabrication.

Among the most effective PCs, there are tandem/cascade cells fabricated using III–V compounds and their solid solutions [12-14]. As a rule, the bottom stage of these cells is made using the GaAs/Ge heterostructure. The investigations of this heterostructure

© 2020, V. Lashkaryov Institute of Semiconductor Physics, National Academy of Sciences of Ukraine

started as early as 1960s, and by now it is quite well-studied. But the interest in the heterostructure is caused by the lattice spatial symmetry match as well as by good agreement of the bond length at the heterointerface. All this allows to utilize GaAs/Ge heterostructure in modern highly efficient PCs.

SLPE technique is a new method. Its theory is not described enough in the literature. As any other technique, SLPE has certain features of its technological stages that one should be aware of to be able to grow quality epitaxial layers of a desired thickness. Thus, in this work we carried out the modelling of epitaxial layer growth by SLPE technique by using, as an example, Ge layer deposition from Ga–Ge solution-melt on GaAs substrate.

2. Theory and modeling

SLPE technique and experimental equipment were described in [11, 15, 16]. To obtain an epitaxial layer by using this technique, a solution-melt should be brought into contact with a cooled substrate for a short period of time. The contact may be realized using the Ampere force. At the end of the growth process the substrate is cleansed immediately of the solution-melt also by using the Ampere force. Thus, the technological stages of SLPE technique are as follows:

1. Heating the growing vessel, homogenization of the solution-melt and the substrate heating, if necessary.
2. Wetting the substrate by the solution-melt.
3. The epitaxial layer growth.
4. Removing the solution-melt from the substrate.

The schematic view of the growing vessel for SLPE used in the simulation of the technological stages is shown in Fig. 1.

Since the first stage is inherent to any other modifications of LPE methods, we have not considered it here and have payed attention to the rest of technological stages. Besides, the above mentioned advantages Ge–GaAs system is also distinguished by high Ge solubility in Ga at low temperatures: about 15 at.% at 500 °C.

2.1. Stress

The contact between the cooled substrate and the solution-melt leads to the initiation of a temperature gradient across the substrate depth. Here, the mechanical stress or strain is formed, which is able to destroy the substrate.

In the first approximation, the strain arising due to non-uniform temperature distribution across the substrate depth during the growth process one can express as follows [17]:

$$\sigma(z,t) = -\frac{E}{1-\nu}\varepsilon(z,t), \tag{1}$$

$$\varepsilon(z,t) = \alpha T(z,t), \tag{2}$$

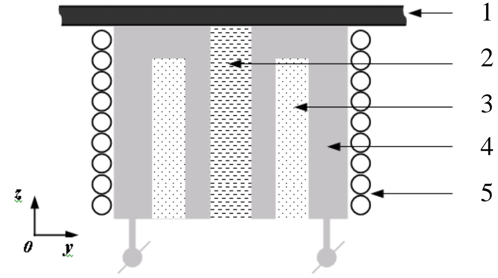

Fig. 1. Schematic view of the growing vessel for scanning liquid phase epitaxy used for modeling. *1* – substrate, *2* – solution-melt in growth capillary, *3* – high-temperature insulator (ceramics), *4* – electrode, *5* – heater.

where E is the Young modulus, GPa; ν – the Poisson ratio; $\varepsilon(z, t)$ – substrate deformation along z-axis with the time lapse; α – thermal expansion coefficient, 1/K [18]; $T(z, t)$ – substrate temperature change along z-axis with the time lapse, K.

For the GaAs substrate one can write the following expression [19]:

$$E = \frac{(c_{11} - c_{12})(c_{11} + 2c_{12})}{c_{11} + c_{12}}, \tag{3}$$

$$\nu = \frac{-c_{12}}{(c_{11} - c_{12})(c_{11} + 2c_{12})} E, \tag{4}$$

where c_{11}, c_{12} are the elastic constants, GPa [20].

By solving the equation (1) with substitution of (2)–(4), it is possible to obtain the strain distribution across the substrate depth (z-axis). Considering the breaking point of the substrate, one can assess minimal possible initial temperature of the substrate T_s (or maximum possible substrate cooling) depending on the initial temperature of the solution-melt T_{sm}. Fig. 2 shows the corresponding calculations.

2.2. Wetting the substrate by the solution-melt and its removal

In the SLPE technique, the processes of wetting of a substrate by a solution-melt and/or the solution-melt removal can be realized using the Ampere force acting on the solution-melt [16]. In this paper, we studied the case where the Ampere force acted from the beginning of the wetting process up to the end of the growth/removal process.

If the substrate is located over the solution-melt (Fig. 1), one should lift the solution-melt against the gravity force to wet the substrate by the solution-melt. But the gap between the substrate and electrodes should not be filled up with the solution-melt. Then the condition of the substrate wetting by the solution-melt can be written as follows:

$$\vec{F}_g < \vec{F}_A \le \vec{F}_g + \vec{F}_c \,, \tag{5}$$

where: $\vec{F}_c, \vec{F}_g, \vec{F}_A$ are the vectors of cohesion, gravity and Ampere forces acting on the solution-melt, respectively.

Expressing (5) in terms of the growing vessel size, it is possible to obtain the value of current to be transmitted through the solution-melt at the given value of magnetic field induction:

$$\rho_{sm} V g < I_w(z) B(z) l_y \sin\alpha \le \rho_{sm} V g + 2\sigma_{sm} L \tag{6}$$

or

$$\frac{\rho_{sm} V g}{B(z) l_y \sin\alpha} < I_w(z) \le \frac{\rho_{sm} V g + 2\sigma_{sm} L}{B(z) l_y \sin\alpha}, \tag{7}$$

$$\rho_{sm} = \rho_{\mathrm{Ga}}(1-x) + \rho_{\mathrm{Ge}} x \,, \tag{8}$$

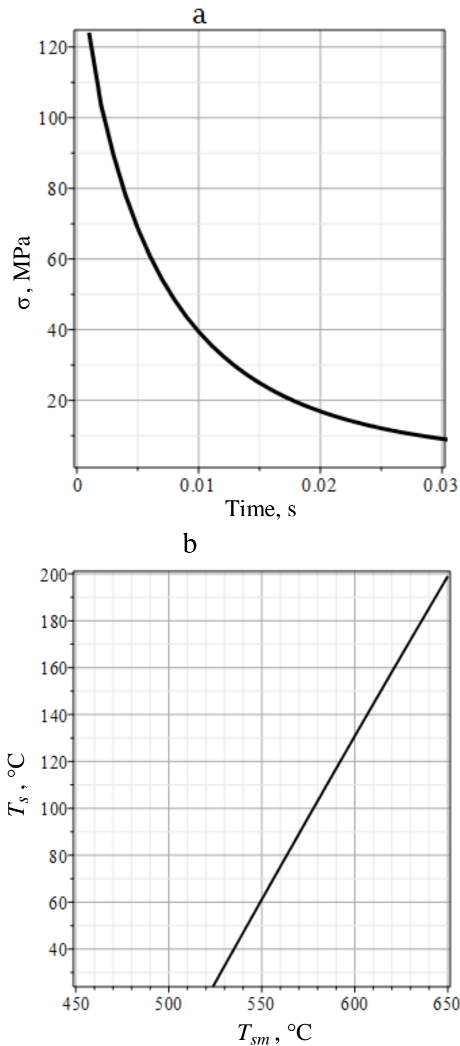

Fig. 2. (a) Dependence of thermally-induced stress on the time t at the crystallization front; (b) dependence of minimal initial temperature of the substrate on the initial temperature of the solution-melt.

where V is the volume of the growth capillary, m^3; g – gravitational acceleration, m/s^2; $I_w(z)$ – total current through the solution-melt to wet the substrate by the solution-melt, A; $B(z)$ – induction of a magnetic field, by which the solution-melt is exposed to, T; l_y – dimension of the solution-melt along y-axis, m; $\sin\alpha = 1$, since the angle between I_w and B is 90°; σ_{sm} – surface tension of the solution-melt, N/m [21]; L – length of the solution-melt contour, m; ρ_{sm}, ρ_{Ga}, ρ_{Ge} are the densities of the solution-melt Ga and Ge, respectively, kg/m^3; x – mole fraction of Ge [22].

Similarly, the condition of the solution-melt removal from the substrate can be written as:

$$\vec{F}_A \ge \vec{F}_g + \vec{F}_a \,, \tag{9}$$

or

$$I_c(z) \ge \frac{-\rho_{sm} V g + \sigma_{sm}(1+\cos\Theta) L}{B(z) l_y \sin\alpha}, \tag{10}$$

where $\vec{F}_a$ is the vector of the solution-melt adhesive force to the substrate; $I_c(z)$ – value of a total current through the solution-melt to cleanse the substrate of the solution-melt, A; Θ – wetting (contact) angle.

In practice, the magnetic field induction can be easily measured and the value of a total current through the solution-melt can be simply calculated. In our opinion, it is more convenient to control the Ampere force by changing the current magnitude to wet and clean the substrate. It is obvious that the current flowing through the solution-melt would cause it, in its turn, an excessive heating – Joule heating. Thus, the value of I_w will be also used for further calculation of a heat transport.

If the contact between the substrate and solution-melt is supposed to break immediately, then the value of I_c does not affect the growth pattern, so this value is of interest only from the technological viewpoint for the substrate cleaning.

2.3. Distribution of the current

In Fig. 1, one can see that due to special shape of the electrodes of the growing vessel the current distribution across the solution-melt depth as well as within the substrate is non-uniform.

To find the current distribution in the solution-melt and in the substrate, we used a two-dimensional model. It is related with the rectangular shape of the growth capillary confined by the high-temperature insulator. Then, the Poisson equation for scalar electrical potential U (Laplace equation) in the two-dimensional case is written as:

$$\frac{\partial^2 U}{\partial y^2} + \frac{\partial^2 U}{\partial z^2} = 0 \,. \tag{11}$$

The current density vector:

$$J_{drift} = -\frac{1}{\rho}\frac{\partial U}{\partial y}, \; J_{diff} = -\frac{1}{\rho}\frac{\partial U}{\partial z} \,. \tag{12}$$

The boundary conditions are:

at external boundaries: $J_n = 0$, (13)

at internal boundaries: $J_n^- + J_n^+ = 0$, (14)

where J_n is the normal component of the current density vector (superscripts "–" and "+" mean the "left" and "right" of the boundary, correspondingly); ρ – resistivity, Ohm·cm.

By solving the systems of equations (7), (8) and (10)–(14), one can find $I_w(y, z)$ and $I_c(y, z)$. The calculation result is shown in Fig. 3.

2.4. The epitaxial layer growth

2.4.1. Heat transport

To investigate the processes of heat transport in the liquid phase and in the substrate the equation of Fourier–Kirchhoff was solved in the following form:

$$\frac{\partial T}{\partial t} = \frac{k}{\rho_{sm} c_p}\left(\frac{\partial^2 T}{\partial x^2} + \frac{\partial^2 T}{\partial y^2} + \frac{\partial^2 T}{\partial z^2}\right) + \frac{I_w^2(y,z)R}{c_p m_{sm}}, \quad (15)$$

where T is the temperature to be found, K; k – heat conductivity coefficient, J/(cm·s·K); c_p – specific heat capacity J/(g·K) [23]; I – current, A; R – resistance, Ohm; m_{sm} – mass of the solution-melt, g; t – time, s; $I_w^2(y,z)R/(c_p m_{sm})$ – component showing additional Joule heating.

Entry conditions. In the initial moment of time, we supposed that the solution-melt and the cooled substrate had different temperatures and the temperature distribution in them was homogenous.

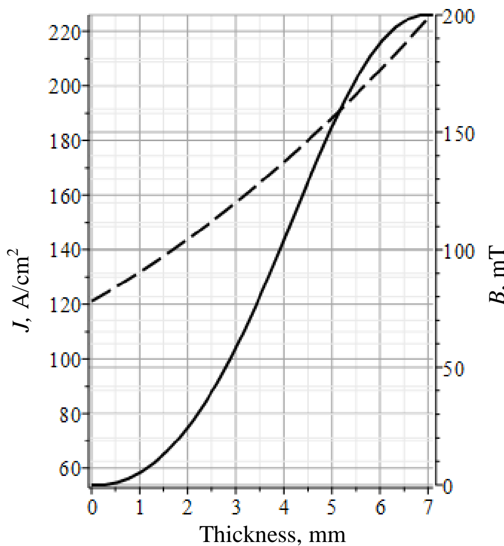

Fig. 3. Height distribution of the current density and the magnetic field induction in the solution-melt at the growth capillary center (curves J (solid line) and B (dashed line)).

Boundary conditions are as follows:

at the top: $k_s \frac{\partial T_s(Z,t)}{\partial z} = a\left(T_s(Z,t) - T_s(Z,0)\right)$,

at the bottom: $T_{sm}(0,t) = T_{sm}(0,0)$, (16)

at the side of the solution-melt:

$$T_{sm}(n,t) = T_{sm}(n-1,t),$$

at the side of the substrate: $T_s(n,t) = T_s(n-1,t)\cdot e^{-\varsigma\cdot h}$,

at the inner boundary: $k_s \frac{\partial T}{\partial z} - k_{sm}\frac{\partial T}{\partial z} = -\pi_{sl} J$, (17)

where π_{sl} is the Peltier coefficient, V; J – current density, A/cm^2; n means the surface normal; $\varsigma = \ln\left[T_s(n,0)/T_s(n-1,t)\right]/\left(\tau 2k\rho/c_p\right)^{0.5}$ – index of the exponent calculated according to the entry conditions and the stability condition of explicit finite-difference scheme; h – step of the finite-difference scheme, cm; τ – total time of the growth process, s.

The heat-transfer coefficient a under the conditions of natural convection can be defined by the following formula:

$$a = 1.3\frac{\mathrm{Nu}\cdot k}{l_b}, \quad (18)$$

where Nu is the Nusselt number; l_b – cooled area length of the substrate, cm; coefficient 1.3 is for a horizontal flat surface giving off the heat upwards.

When the number Ra < 500:

$$\mathrm{Nu} = 1.18\mathrm{Ra}^{0.125}\left(\frac{\mathrm{Pr}_g}{\mathrm{Pr}_s}\right)^{0.25}, \quad (19)$$

where Ra is the Rayleigh number; Pr is the Prandtl number taken according to the reference data for a given temperature ("g" and "s" subscripts stand for "gas" and "surface" of a substrate, correspondingly).

$$\mathrm{Ra} = \mathrm{Gr}\cdot \mathrm{Pr}_g, \quad (20)$$

$$\mathrm{Gr} = \frac{g\cdot\beta\cdot\left(T_s(Z,t) - T_s(Z,0)\right)\cdot l_b^3}{\nu^2}, \quad (21)$$

$$\mathrm{Pr}_g = \frac{\nu}{a_T}, \quad (22)$$

where Gr is the Grashof number; $\beta = 1/T$ – coefficient of cubical expansion of gas, 1/K; $\nu = \eta/\rho_{sm}$ – coefficient of kinematic viscosity of gas, cm^2/s; η – coefficient of dynamic viscosity of gas, N·s/cm^2; $\alpha_T = k/(\rho\cdot c_p)$ – thermal diffusivity, cm^2/s.

To solve the equation (15) with entry and boundary conditions (16), (17), we used the method of finite differences. The calculation results are shown in Figs 4 and 5.

2.4.2. Mass transport

The characteristic feature of SLPE technique is a short-time contact between a solution-melt and a substrate with $\tau \leq 1$ s. In this case, the growth mode can be considered as the diffusion one. *I.e.*, the convective component of the mass transport may be neglected in viscous fusible metal-solvent. For the growing vessel the proposed characteristic time of diffusion is as follows:

$$\tau_D = \frac{l^2}{D_l} \approx 10^4 \text{ s}, \tag{23}$$

where l is the height of the solution-melt over/under the substrate (~1 cm).

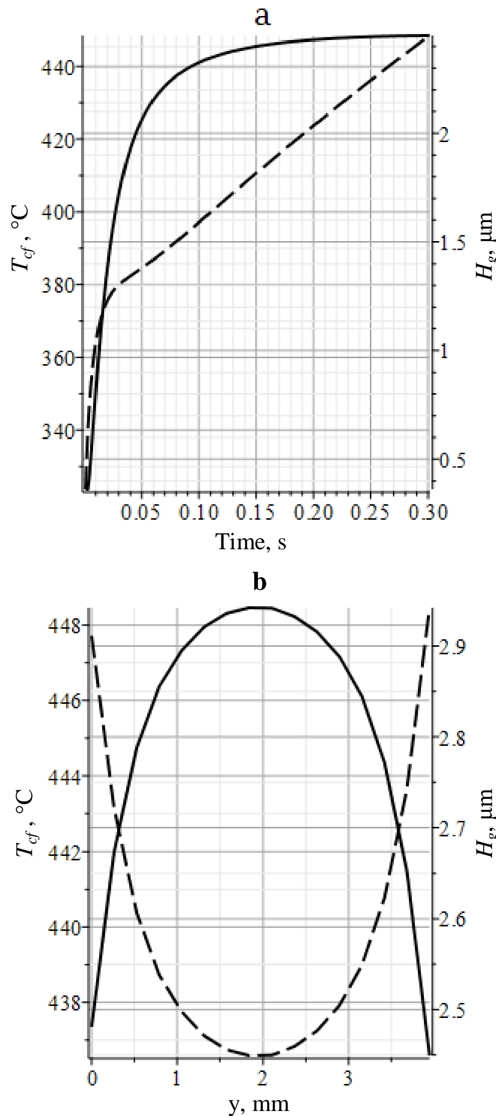

Fig. 4. (a) Dependence of the crystallization front temperature and the layer thickness on the time (curves T_{cf} (solid line) and H_g (dashed line), respectively); (b) temperature distribution at the crystallization front and the layer thickness distribution depending on the growing vessel width in the direction of the current flow (curves T_{cf} (solid line) and H_g (dashed line), respectively).

This makes much more time than the process time itself, *i.e.*, $\tau_D >> \tau$. Thus during the time of an epitaxial layer growth the concentration change of a component being deposited near the substrate does not affect the concentration at the opposite side of solution-melt. In this case, there is a growth from a semi-infinite solution-melt [23].

Summarizing all the aforesaid, one can write the equation of mass transport (2nd Fick law) for SLPE:

$$\frac{\partial N}{\partial \tau} = D_l \left(\frac{\partial^2 N}{\partial x^2} + \frac{\partial^2 N}{\partial y^2} + \frac{\partial^2 N}{\partial z^2} \right) - \mu E \frac{\partial N}{\partial y}, \tag{24}$$

where D_l is the interdiffusion coefficient of a component, cm²/s [23]; μ – mobility of Ge, cm²/(V·s); $E = J_{w(y,\,z)} \cdot \rho$ – electric field, V/cm.

Entry conditions. We assumed that the solution-melt was homogenized before every growth act. Thus in the initial moment of time the dissolved component concentration distribution in the solution-melt is uniform and corresponds to the equilibrium concentration at the initial temperature of the solution-melt.

Boundary conditions (at the exterior boundaries) had the form:

$$\begin{aligned} &\text{at the top:} && N(x, y, Z, t) = N_e\left(T_{cf}(x, y, t)\right), \\ &\text{at the bottom:} && N(x, y, 0, t) = N_e(t = 0), \\ &\text{at the side:} && N(n, t) = N(n-1, t), \end{aligned} \tag{25}$$

where N_e is the equilibrium concentration; T_{cf} – temperature at crystallization front.

For the Ga–Ge system [23]:

$$N\ (x, y, z, t) = \frac{N_A \cdot \rho_{sm} \cdot x(x, y, z, t)}{M_{Ga}(1 - x(x, y, z, t)) + M_{Ge} x(x, y, z, t)}, \text{cm}^{-3}, \tag{26}$$

where N_A is the Avogadro number, mole^{-1}; M_{Ga}, M_{Ge} are the molar masses of Ga and Ge respectively, g/mole.

The thickness of epitaxial layer being deposited was calculated using the formula:

$$H_g(x, y, t) = \frac{10^4 \cdot 2 \cdot \Delta N_l^{\Sigma}(x, y)}{N_S \cdot \pi^{0.5}} (D_l\, t)^{0.5}, \ \mu\text{m}, \tag{27}$$

where N_s is the component concentration in the solid phase, cm^{-3}; ΔN_l^{Σ} – sum of differences between the initial and the final equilibrium component concentration (or oversaturation) in the solution-melt within the time considered, cm^{-3}; t – time, s.

Simultaneously solving the equations (24)–(27) with substitution of the obtained above data on the temperature and current distributions, one can find the thickness of the grown epitaxial layer. The calculation results are shown in Figs 4 and 5. The parameters necessary for calculation are presented in the table.

Table. Input parameters.

Parameter	Unit	Value
Growth capillary size	mm	3.9×3.9×7.1
Substrate thickness	μm	395
The size of electrode part adjacent to the solution-melt	mm	3.9×2.1×7.1
Θ	degree	28
π_{sl}	V	0.3

3. Results of modeling and discussion

3.1. Stress

Thermally-induced stress arising in a cold substrate during the contact with a hot solution-melt was calculated. The stress is maximal at the crystallization front and exponentially decays with the time lapse (see Fig. 2a). So, the initial moment of the contact between the cold substrate and the hot solution-melt is the very moment to be considered. Fig. 2b shows the calculation of the initial temperature inherent to the substrate, which depends on the initial temperature of the solution-melt. To calculate, the following requirements were put on: the stress arising in the initial moment of time should not damage the substrate and must be less than the breaking point for GaAs (150 MPa). The latter figure shows that for the chosen growth temperature (500 °C) the substrate might have the near room temperature 25 °C.

3.2. Wetting the substrate with the solution-melt and its cleaning

The calculated values of the total current through the solution-melt to wet the substrate and to clean it are: 11 A $< I_w <$ 41 A and $I_c \geq$ 39 A, respectively.

We should note that the obtained current values were calculated for the above mentioned parameters of the growth process (growth temperature, solution-melt and substrate composition) and the growing vessel size. Fig. 3 (curve *J*) shows the height distribution of the current in the solution-melt (z-axis) at the growth capillary. The calculation showed a weak current change along the y-axis. We believe that it is caused by the current spreading into the substrate. The gradient of magnetic field induction accepted for the calculations is shown in Fig. 3 (curve *B*).

The gradient distribution of these values in the solution-melt (z-axis) and in the substrate arises due to the special shape of the electrodes in the growing vessel (see Fig. 1). As a result, the maximal current and maximal magnetic field will be at the crystallization front where the substrate cleaning of the solution-melt takes place. In addition, it will allow to decrease “unwanted” Joule heating of the solution-melt bottom.

3.3. Heat transport

Fig. 4a (curve T_{cf}) shows that the overcooling at the growth interface decreases substantially with the time lapse and later remains almost constant. As it has been mentioned above, the characteristic feature of our technique is a short-time contact between the solution-melt and substrate. Thus, the effective contact time between the substrate and solution-melt should be $t \leq 0.3$ s. If the contact time reaches $t > 0.3$ s, then one should consider that there is a growth in a temperature gradient.

Fig. 4b (curve T_{cf}) shows that there is non-linear and asymmetric (with respect to y-axis) temperature change at the crystallization front in the direction of the current flow. We believe it is connected with two factors: the heat spreading into the cold substrate and Peltier effect. The effect is caused by spreading of the current into the substrate. And where the current enters the substrate, there is the crystallization front cooling, while where the current exits the substrate there is the crystallization front heating. The result of Peltier effect action can be seen in Fig. 4b (curve T_{cf}) – there is a small temperature difference at the area boundaries. The temperature change along the x-axis is related only with the heat spreading into the substrate (Fig. 5a). In Figs 4b and 5a, one can see that the biggest contribution into the temperature change at the crystallization front is made by the heat spreading into the cold substrate.

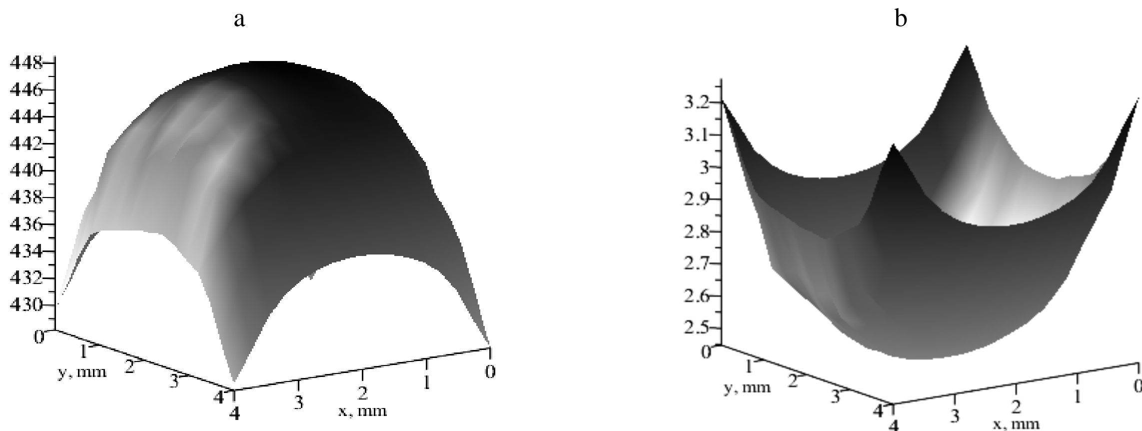

Fig. 5. (a) Temperature distribution at the crystallization front; and (b) the layer thickness distribution over the substrate surface.

3.4. Mass transport

The calculated thickness of the grown epitaxial layer depending on the above mentioned conditions is shown in Figs 4 and 5b. Fig. 4a (curve H_g) shows that after 0.03 s, the epitaxial layer thickness changes linearly in spite of the non-linear temperature change. In our opinion, it is related with the sustained concentration profile in the solution-melt.

In Fig. 4b (curve H_g), one can see that the heat spreading into the cold substrate contributes about 25% into the change of the epitaxial layer thickness over the surface. Peltier effect contribution in the whole growth pattern is minor – less than 1% of change of the epitaxial layer thickness over the surface. Fig. 5b presents the whole growth pattern confirming the mentioned above.

During the calculations, we assumed that wetting the substrate by the solution-melt was achieved by means of the Ampere force. *I.e*., the current flows through the solution-melt and the substrate and produces Joule heating – equation (15). To reveal the influence of Joule heating on the growth pattern, we carried out the simulation with Joule heating component and without it in equation (15). Comparing the results, we found that Joule heating contributed into change/increment of the epitaxial layer thickness about +0.7%. Obviously, the Joule heating component becomes more essential when using large mass of the solution-melt, which causes applying larger currents to obtain the larger Ampere force necessary for wetting the substrate by the solution-melt. Also, significant increase of the current through the solution-melt will lead to the overcooling decrease at the crystallization front till the overcooling disappearance and the beginning of the substrate dissolution. Simultaneously, the contribution of Peltier effect will be increased.

To reveal the influence of electromigration on the growth pattern, we carried out simulation with electromigration component and without it in the equation (24). Comparing the results we did not found any influence of electromigration on the grown epitaxial layer thickness. We believe such a result is related with low electric mobility of Ge in Ga and with very small growth time.

4. Conclusions

The mathematic model of technological stages of SLPE technique depending on the technological parameters of the growth process was created. Being based on the example of modelling of the technological stages of Ge epitaxial layers growing on GaAs substrate from Ga–Ge solution-melt by using SLPE technique, we showed that:

- it is necessary to heat the substrate to avoid its destruction at the growth temperatures above 530 °C;
- Peltier effect and Joule heating almost do not affect the growth pattern. Peltier effect can be decreased using high-resistance substrates. Joule heating can be also lowered by decreasing the solution-melt size and the growth time;
- the electromigration and the convection in the solution-melt may be neglected due to the short-time contact between the substrate and the solution-melt;
- the whole growth pattern is affected by: initial process parameters (initial temperature and sizes of the substrate and the solution-melt), conditions of the heat removal from the substrate back side and the process time itself;
- heat spreading in the cold substrate contributes the most into the thickness distribution of the epitaxial layer over the substrate surface.

References

1. R. Kour, S. Arya, S. Verma *et al.* Review – Recent advances and challenges in indium gallium nitride ($In_xGa_{1-x}N$) materials for solid state lighting. *ECS J. Solid State Sci. Technol.* 2020. **9**. 015011. https://doi.org/10.1149/2.0292001JSS.
2. Izyumskaya N., Avrutin V., Ding K. *et al.* Emergence of high quality sputtered III-nitride semiconductors and devices. *Semicond. Sci. Technol.* 2019. **34**. 093003. https://doi.org/10.1088/1361-6641/ab3374.
3. Niu S., Wei Z., Fang X. *et al.* Brief review of epitaxy and emission properties of GaSb and related semiconductors. *Crystals*. 2017. **7**. P. 337. https://doi.org/10.3390/cryst7110337.
4. Ci J.-W., Lian C.-Y., Uen W.-Y. *et al.* Formation mechanism of high Ge content SiGe epilayer on Si by liquid phase epitaxy using Ge–Sn solution. *Thin Solid Films.* 2020. **704**. P. 137981. https://doi.org/10.1016/j.tsf.2020.137981.
5. Zhang D., Yang Q., Jiang Y. *et al.* Laser-induced damage of garnet films grown by LPE. *Opt. Mater*. 2019. **91**. P. 268–273. https://doi.org/10.1016/j.optmat.2019.03.034.
6. Wang Y., Hu S., Zhou W. *et al.* LPE growth and optical characteristics of $GaAs_{1-x}Sb_x$ epilayer. *J. Cryst. Growth*. 2017. **463**. P. 123–127. https://doi.org/10.1016/j.jcrysgro.2017.01.040.
7. Ashery A., Farag A.A.M. Fabrication, structural and electrical characterization of $AlNi_2Si$ based heterojunction grown by LPE. *Materials Science in Semiconductor Processing*. 2015. **35**. P. 66–74. https://doi.org/10.1016/j.mssp.2015.02.052.
8. Tsybrii Z., Bezsmolnyy Yu., Svezhentsova K. *et al.* HgCdTe/CdZnTe LPE epitaxial layers: From material growth to applications in devices. *J. Cryst. Growth*. 2020. **529**. P. 125295. https://doi.org/10.1016/j.jcrysgro.2019.125295.
9. Donchev V., Milanova M., Georgiev S., Kostov K.L., Kirilov K. Dilute nitride InGaAsN and GaAsSbN layers grown by liquid-phase epitaxy for photovoltaic applications. *J. Phys.: Conf. Series*. 2020. **1492**. P. 012049. https://doi.org/10.1088/1742-6596/1492/1/012049.

10. Tsybulenko V.V., Shutov S.V., Maronchuk A.I. Analysis of conditions for obtaining thin and ultrathin epitaxial layers by liquid-phase epitaxy. *Proc. 15th Intern. scientific-practical conf. "Modern information and electronic technologies"*. Ukraine. Odessa. May 26–30, 2014. II. P. 132.
11. Tsybulenko V.V., Shutov S.V., Yerochin S.Yu. LPE application technique for obtaining of thin film semiconductor materials. *Proc. 1st Intern. Electronic Conf. on Crystals* (IECC 2018). May 21–31, 2018. https://doi.org/10.3390/IECC_2018-05250.
12. Lan D., Green M. Up-conversion of sunlight by GaInP/GaAs/Ge cell stacks: Limiting efficiency, practical limitation and comparison with tandem cells. *Energy Procedia*. 2017. **130**. P. 60–65. https://doi.org/10.1016/j.egypro.2017.09.396.
13. Theristis M., O'Donovan T.S. Electrical-thermal analysis of III–V triple-junction solar cells under variable spectra and ambient temperatures. *Solar Energy*. 2015. **118**. P. 533–546. https://doi.org/10.1016/j.solener.2015.06.003.
14. Kim D.-S., Jeong Y., Jeong H., Jang J.-H. Triple-junction InGaP/GaAs/Ge solar cells integrated with polymethyl methacrylate subwavelength structure. *Appl. Surf. Sci*. 2014. **320**. P. 901–907. https://doi.org/10.1016/j.apsusc.2014.09.138.
15. *Patent of Ukraine UA 93097 U*, CI (2014.01) C30B 19/00. A method of producing epitaxial layers of the liquid phase. V.V. Tsybulenko, S.V. Shutov, O.V. Yevdokymov, O.O. Boskin. u201313247, appl. 14.11.2013. Publ. 25.09.2014, Bull. No 1.
16. *Patent of Ukraine UA 115873 C2*, CI (2006), C30B 19/00, H01L 21/208, H01L 21/20 (2006.01). A method of wetting of substrate and its purification from solution-melt during liquid phase epitaxy. V.V. Tsybulenko, S.V. Shutov, S.Yu. Yerochin. a201408609, appl. 28.07.2014. Publ. 10.01.2018, Bull. No 1.
17. Milvidsky M.G., Osvensky V.B. *Structural Defects in Semiconductors Epitaxyal Layers*. Moscow: Metallurgiya. 1985. P. 10 (in Russian).
18. Yang V.K., Groenert M., Leitz C.W. *et al.* Crack formation in GaAs heteroepitaxial films on Si and SiGe virtual substrates. *J. Appl. Phys.* 2003. **93**, No 7. P. 3861. https://doi.org/10.1063/1.1558963.
19. Shuvalov L.A. (Ed.) *Modern Crystallography IV: Physical Properties of Crystals.* Springer Science & Business Media, 2012. P. 66. https://doi.org/10.1007/978-3-642-81838-7.
20. http://www.ioffe.ru/SVA/NSM/Semicond/GaAs/mechanic.html
21. Chentsov V.P., Shevchenko V.G., Mozgovoy A.G., Pokrasin M.A. Density and surface tension of heavy liquid-metal coolants: Gallium and indium. *Inorganic Materials: Appl. Res*. 2011. **2**, No 5. P. 468–473. https://doi.org/10.1134/S2075113311050108.
22. *State Diagrams of Double Metal Systems*. Book 2. Lyakishev N.P. (Ed.) Moscow: Mashinostroenie. 2000. P. 593 (in Russian).
23. Sokolov I.A. *Calculations of Semiconductor Technology Processes.* Moscow: Metallurgiya. 1994. P. 96 (in Russian).

Визначення умов кристалізації гетероструктур Ge/GaAs у методі скануючої рідиннофазної епітаксії

В.В. Цибуленко, С.В. Шутов, С.Ю. Єрохін

Анотація. Ми провели моделювання окремих технологічних етапів скануючої рідиннофазної епітаксії (СРФЕ): змочування підкладки розчином-розплавом за допомогою сили Ампера, вирощування епітаксійного шару під час короткочасного контакту між підкладкою і розчином-розплавом та видалення розчину-розплаву з підкладки з використанням сили Ампера. Моделювання проводили для випадку вирощування шарів Ge на підкладці GaAs з розчину-розплаву Ga-Ge при температурі 500 °C. Було виявлено, що ефект Пельтьє та джоулево тепло практично не впливають на структуру росту та за певних умов їх навіть можна зменшити. Електроміграцією та конвекцією у розчині-розплаві можна знехтувати. Показано, що основними технологічними параметрами методу СРФЕ є такі: початкові температури та розміри підкладки і ростової комірки, умови відведення тепла з тильного боку підкладки та час процесу росту. Було також показано, що основним внеском у розподіл товщини епітаксійного шару по поверхні підкладки був розподіл тепла в охолодженій підкладці.

Ключові слова: скануюча рідиннофазна епітаксія, сила Ампера, гетероструктури, тонкі плівки.